# Accuracy of substrate selection by enzymes is controlled by kinetic discrimination

Kinshuk Banerjee,[†] Anatoly B. Kolomeisky,[*,†,‡] and Oleg A. Igoshin[*,†,¶]

[†]*Center for Theoretical Biological Physics, Rice University*

[‡]*Dept. of Chemistry, Rice University*

[¶]*Dept. of Bioengineering, Rice University*

E-mail: tolya@rice.edu; igoshin@rice.edu

**Abstract**

Enzymes have the remarkable ability to select the correct substrate from the pool of chemically similar molecules. The accuracy of such a selection is determined by differences in the free energy profiles for the right and wrong reaction pathways. Here, we investigate what features of the free energy landscape govern the variation and minimization of selectivity error. It is generally believed that minimal error is affected by both kinetic (activation barrier heights) and thermodynamic (binding stability) factors. In contrast, using first-passage theoretical analysis, we show that the selectivity error is only determined by the differences in transition state energies between the pathways and independent of the energies of the stable complexes. The results are illustrated for two common catalytic mechanisms (i) the Michaelis-Menten scheme and (ii) an error-correcting kinetic proofreading scheme with tRNA selection and DNA replication as guiding biological examples. Our theoretical analysis therefore suggests that the selectivity mechanisms are always kinetically controlled.

# Graphical TOC Entry

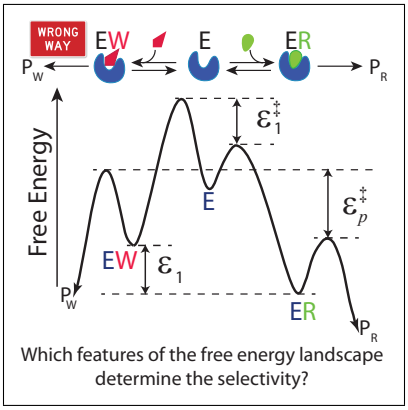


# Keywords

Enzyme kinetics, Free energy landscape, Proofreading

Enzymes are biological catalysts that are essential for all processes in living organisms. They exhibit extraordinary accuracy in selecting for the right (cognate) substrate and against the wrong (near/non-cognate) ones. For example, the enzymes involved in all the stages of biological information processing – replication, transcription and translation, show remarkable fidelity.[1,2] It is widely believed that the selectivity of an enzyme is due to the difference in the free energy profiles for two types of substrates giving desirable and undesirable products. Given finite (and often small) free energy differences for chemically-similar substrates, there must be a lower limit of the error, $\eta$, the enzymes can achieve.

Interestingly, there are contrasting views on the condition under which the minimal error is achieved. Several studies, including the seminal work by Hopfield on enzyme selectivity,[3] suggest that the minimum error, $\eta_{\rm min}$, is obtained when the catalytic rate tends to zero. On the other hand, some other investigations, *e.g.*, the study on co-polymerization by Bennett,[4] argue for the opposite case: the lowest error is achieved for very fast catalytic rates. A recent work by Sartori *et al.*[5] reconciled these opposing results by suggesting that there are two mechanisms of enzymatic discrimination: kinetic (difference in activation barrier heights dominates) and energetic (difference in binding stability of intermediates dominates). Taking the Michaelis-Menten(MM) enzyme kinetic scheme, it was shown that for kinetic discrimination, $\eta_{\rm min}$ is obtained at very fast catalytic rate whereas for energetic discrimination, $\eta_{\rm min}$ is attained when the catalytic rate tends to zero. The Hopfield approach takes equal binding rate constants for right (R) and wrong (W) substrates but different equilibrium constants. As there is no difference in barrier heights, the discrimination is energetic. The Bennett scheme, on the other hand, with different binding and dissociation rate constants but the same equilibrium constant (zero difference in intermediate stability) employs the kinetic discrimination. Hence, both the situations are limiting cases of a more general selectivity mechanism where binding and dissociation rate constants as well as the equilibrium constants can be different between the R and W pathways.[5]

However, there is a crucial simplifying assumption in the study of Sartori *et. al.*,[5] which

is the equality of the catalytic rate constants for both right and wrong pathways. Such assumptions are also present in more general models of enzyme accuracy[6,7] that consider kinetic proofreading (KPR), a non-equilibrium error-correcting mechanism in biological processes. This is the mechanism that was proposed independently by Hopfield[3] and Ninio[8] to explain the strikingly low errors in different biological polymerization processes, and it was later verified experimentally in different biochemical systems.[9–11] Now, in contrast to these theoretical views, experimental kinetic data on biological KPR networks, *e.g.*, in DNA replication[11] and peptide chain elongation[12] suggest that catalytic rates are significantly higher for the right pathway. Hence, the theoretical study of the selectivity mechanisms even in the basic MM scheme should be more realistic by considering these rates different. Similar considerations can be applied to the classical Hopfield-Ninio(HN) KPR model[3] where only the dissociation rate constants of the intermediates are taken to be different between the two pathways. Then, for given differences in the free-energy profiles between the right and wrong pathways, we ask the following questions: (i) What features of the free energy landscapes in such complex biochemical systems determine the value of the selectivity error? (ii) How does the error change with the kinetic parameters and how many different patterns of error variation can be observed? and (iii) Out of various theoretical possibilities, which patterns of error variation are realized in living systems?

We theoretically analyze the enzymatic selectivity by considering the overall process as a first-passage problem.[13] **The standard definition of selectivity error $\eta$ is given as the ratio of the steady-state flux of wrong product formation to that of the right product formation.[3] In our methodology, this is given in terms of the ratio of the splitting probability of reaching the wrong end(product) to that of reaching the right end where the end states are absorbing states. These probabilities are determined from the respective first-passage probability densities to reach either end for the first time before reaching the other, starting from the free enzyme state E (see Fig. 1(a)). Detailed calculations are given in the SI.**

**The first-passage approach, of course, yields the same expression for error as obtained from the steady-state fluxes. We note that, along with splitting probabilities, other dynamic properties of the system can be obtained by solving the time-evolution equations of the first-passage probability densities, also called the backward master equations.[13,14] Our focus here is on the selectivity error.**

We begin our analysis with the MM scheme shown in Fig. 1(a). For this scheme our analytical calculations give the following expression for the selectivity error in terms of the rate constants (see Fig. 1(a))

$$\eta = \left(\frac{k_{p,W}/K_{M,W}}{k_{p,R}/K_{M,R}}\right) = f_1 f_p \left(\frac{k_{p,R}+k_{-1,R}}{f_p k_{p,R} + f_{-1}k_{-1,R}}\right) = f_1 \left(1 + \frac{\frac{f_p}{f_{-1}} - 1}{1 + \frac{f_p}{f_{-1}}\frac{k_{p,R}}{k_{-1,R}}}\right) \tag{1}$$

where $f_i = k_{i,W}/k_{i,R}$, $(i = \pm 1, p)$ and $K_{M,R/W} = \frac{k_{-1,R/W}+k_{p,R/W}}{k_{1,R/W}}$ is the MM constant. The factors $f_i$ play important role in our analysis. They are related to the free energy discriminations (in units of $k_{\rm B}T$) between the respective states of the two pathways (see Fig. 1(b)): $f_1 = e^{-\varepsilon_1^\ddagger}$, $f_{-1} = e^{(\varepsilon_1 - \varepsilon_1^\ddagger)}$, $f_p = e^{(\varepsilon_1 - \varepsilon_p^\ddagger)}$. The limits of error when catalysis rate is low ($k_{p,S} << k_{-1,S}$, $S = R/W$, $f_p$ fixed) and high ($k_{p,S} >> k_{-1,S}$, $f_p$ fixed) are given by

$$\eta_{\rm L} = \frac{f_1 f_p}{f_{-1}} = e^{-\varepsilon_p^\ddagger};\ \eta_{\rm H} = f_1 = e^{-\varepsilon_1^\ddagger};\ \frac{\eta_{\rm L}}{\eta_{\rm H}} = \frac{f_p}{f_{-1}} = e^{(\varepsilon_1^\ddagger - \varepsilon_p^\ddagger)}. \tag{2}$$

Three important conclusions can be made by analyzing Eqs.(1) and (2). First, the error only depends on the values of transition-state energy differences (kinetic factors) $\varepsilon_j^\ddagger$ $(j = 1, p)$ and independent of $\varepsilon_1$, i.e. $\frac{\partial \eta}{\partial \varepsilon_1} = 0$. This can be seen from the fact that both numerator and denominator in the ratios $\frac{f_p}{f_{-1}}$ and $\frac{k_{p,R}}{k_{-1,R}}$ have the same $\varepsilon_1$ scaling making the ratios invariant to its changes (See SI for more discussion). **We point out that we have assumed equal frequency factors for all the rate constants. However, our conclusion will remain valid even if they are different but their ratio is independent of $\varepsilon_1$.** Second, the

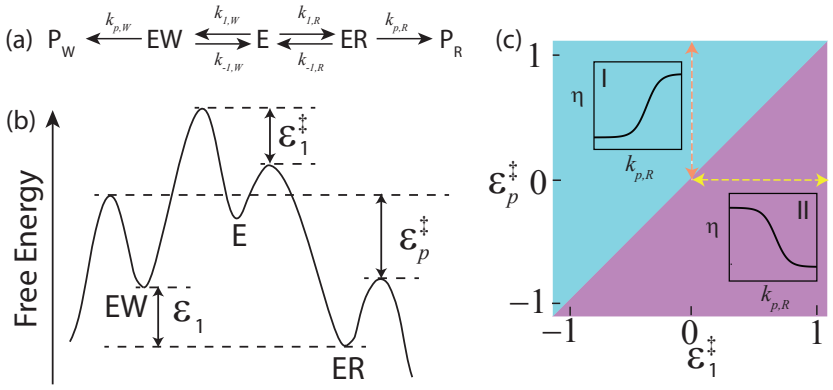


Figure 1: (a) A schematic view of the reaction network with right (R) and wrong (W) substrates being transformed into respective products by enzyme E. The catalysis is based on MM kinetics with distinct rate constants for all the steps between the R and W pathways. (b) Free energy profile of the network in panel (a) with the energy differences between the pathways highlighted. The difference in transition state energies are denoted by $\varepsilon_j^\ddagger$ $(j = 1, p)$ and $\varepsilon_1$ is the binding stability difference of the intermediates. (c) A phase diagram showing two different regimes of error, $\eta$, variation with the catalytic rate constant $k_{p,R}$ ($f_p$ fixed) as predicted from Eq.(2). The Hopfield-like case lies along the vertical orange dashed arrow whereas, the pattern for Bennett scheme lies along the horizontal yellow dashed arrow.

error changes monotonically with the catalytic rate constant $k_{p,R}$ (with other parameters including $f_p$ fixed); this can be easily seen from the last expression in Eq.(1). The sign of the slope is given by the sign of $(\frac{f_p}{f_{-1}} - 1)$ or equivalently the sign of $\varepsilon_1^\ddagger - \varepsilon_p^\ddagger$. Third, the limiting values of the error are given by $\eta_{\min} = \eta_{\rm L}(\eta_{\rm H})$ for $\varepsilon_1^\ddagger < \varepsilon_p^\ddagger$ $(\varepsilon_1^\ddagger > \varepsilon_p^\ddagger)$. These properties of the error variation are shown in a phase digram in Fig. 1(c). It can be easily seen from Eq.(1) that the same monotonic behavior of error is obtained as a function of $k_{-1,R}$ (keeping $f_{-1}$ fixed) but with a flip between increasing and decreasing behaviors and between low and high value limits.

To reconcile these results with others, we note that the Bennett scheme is reproduced from Eq.(2) when $\varepsilon_1^\ddagger > 0$, $\varepsilon_p^\ddagger = 0 = \varepsilon_1$ and hence, $\eta_{\min}$ is achieved at very high $k_{p,S}$. The corresponding pattern is found along the horizontal yellow dashed arrow in Fig. 1(c). In contrast, one recovers the Hopfield scenario by setting $\varepsilon_1^\ddagger = 0$, $\varepsilon_p^\ddagger = \varepsilon_1 (> 0)$ (the vertical orange dashed arrow in Fig. 1(c)). Then, $\eta_{\min}$ is obtained when $k_{p,S}$ tend to zero, as expected. It is important to note that in this special case, the kinetic discrimination $\varepsilon_p^\ddagger$ coincides

with the thermodynamic discrimination $\varepsilon_1$. Here and in what follows, we use the term 'thermodynamic discrimination' in the same meaning as in 'energetic discrimination' used by Sartori *et al.*[5] We emphasize, that general independence of the error value on the energies of ER and EW complexes, and hence on their difference, indicates *kinetic discrimination always controls the selectivity error* for MM scheme.

To check the validity of these conclusions in a more general setting, we analyze a single-loop proofreading scheme that comes with two intermediates as shown in Fig. 2(a). It can also be straightforwardly analyzed using the first-passage technique. The correspond-

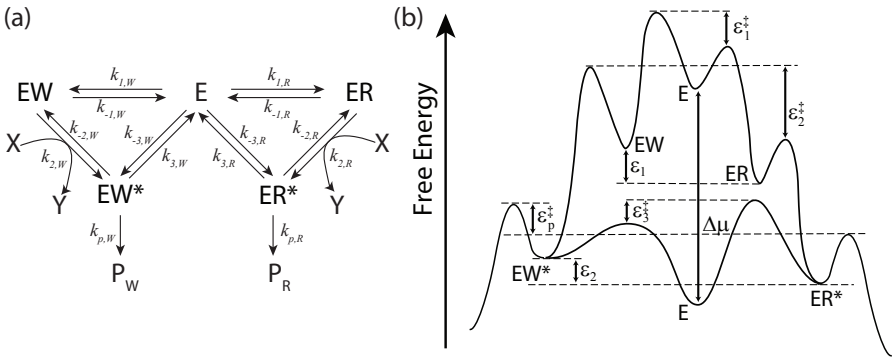


Figure 2: (a) A schematic view of the general one-loop KPR reaction network. X is some energy-currency molecule (like ATP) and Y is its hydrolyzed product (like ADP+Pi). (b) Corresponding free energy landscape with the energy discriminations between the pathways shown. The chemical potential difference over the cycles $\Delta\mu = \mu_{\rm X} - \mu_{\rm Y}$.

ing free energy landscape highlighting the energy differences in various steps is depicted in Fig.2(b). The discrimination factors defined as $f_i = k_{i,W}/k_{i,R}$, $(i = \pm1, \pm2, \pm3, p)$ can be expressed in terms of the discrimination energy parameters: $f_2 = e^{(\varepsilon_1 - \varepsilon_2^\ddagger)}$, $f_{-2} = e^{(\varepsilon_2 - \varepsilon_2^\ddagger)}$, $f_3 = e^{(\varepsilon_2 - \varepsilon_3^\ddagger)}$, $f_{-3} = e^{-\varepsilon_3^\ddagger}$, $f_p = e^{(\varepsilon_2 - \varepsilon_p^\ddagger)}$ ($f_{\pm1}$ are defined as in the MM case). Taking step-2 and step-3 to be strongly driven forward ($k_{-3,S} << k_{1,S}$, $k_{-2,S} << k_{3,S}$, $S = R/W$), we obtain the following expression for the error (for general expression, see SI )

$$\eta = f_1 f_2 f_p \left( \frac{\gamma + k_{3,W}/k_{-2,W}}{\gamma + k_{3,R}/k_{-2,R}} \right) \left( \frac{k_{-1,R} + k_{2,R}}{k_{-1,W} + k_{2,W}} \right) \left( \frac{k_{3,R} + k_{p,R}}{k_{3,W} + k_{p,W}} \right). \tag{3}$$

The quantity $\gamma$ is related to the chemical potential difference, $\Delta\mu$ (in units of $k_{\rm B}$T) over the

R (or W) cycle by $\gamma = \prod_{i=1}^{3} \frac{k_{i,R}}{k_{-i,R}} = \prod_{i=1}^{3} \frac{k_{i,W}}{k_{-i,W}} = e^{\Delta\mu}$. Since $\Delta\mu$ is the same for the two cycles, discrimination factors are constrained by $\prod_i \frac{f_i}{f_{-i}} = 1$.

As in MM case, both the approximate value of error (Eq. (3)) and the exact expression (given in SI) are invariant with respect to changes in stability of ER, EW, ER* and EW* as long as difference in transition state energies $\varepsilon_i^{\ddagger}$ and $\Delta\mu$ are fixed, *i.e.*, $\frac{\partial\eta}{\partial\varepsilon_1} = \frac{\partial\eta}{\partial\varepsilon_2} = 0$ (see SI for details). Moreover, it follows from Eq.(3) that error variation is a monotonic function of $k_{p,R}$ (compare with Eq.(1), $f_p$ fixed). The sign again is determined by the sign of $\varepsilon_3^{\ddagger} - \varepsilon_p^{\ddagger}$. The ratio of the high and low $k_{p,R}$ limits comes out as (see SI) $\eta_{\rm L}/\eta_{\rm H} = f_p/f_3 = e^{(\varepsilon_3^{\ddagger} - \varepsilon_p^{\ddagger})}$. For $\varepsilon_3^{\ddagger} < \varepsilon_p^{\ddagger}$ , one has $\eta_{\rm min} = \eta_{\rm L}$ whereas for $\varepsilon_3^{\ddagger} > \varepsilon_p^{\ddagger}$, $\eta_{\rm min} = \eta_{\rm H}$ (see Eq.(2) for comparison). Thus, only transition state energy differences dictate the value of the error and condition under which minimal error is achieved. In the HN model of proofreading[3] the authors assumed $f_p = 1,\ f_3 > 1$. Thus, in this case the minimum error can only be obtained when the catalytic rate is very low.

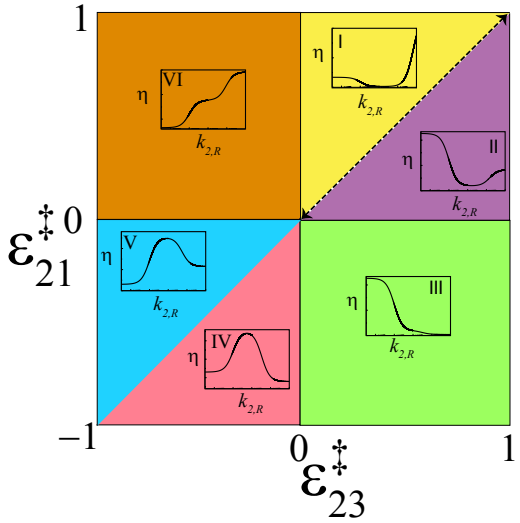


Figure 3: A phase diagram displaying six regions of distinct error variation patterns. The curves are generated as a function of $k_{2,R}$ (fixed $f_2$) with the following choice of model rate parameters: $k_{1,R} = 5.0$, $k_{-1,R} = 50.0$, $k_{3,R} = 1.0$, $k_{-2,R} = 10^{-3}$, $k_{-3,R} = 10^{-3}$, $k_{p,R} = 10^{-2}$ (all in $s^{-1}$). The energetic discriminations are taken as (in units of $k_{\rm B}T$): $\varepsilon_1 = 4.0$, $\varepsilon_2 = 5.0$, $\varepsilon_2^{\ddagger} = 5.5$. The curves representing the patterns for regions I-III are determined by setting $\varepsilon_3^{\ddagger} = 3.0$ and varying the parameter $\varepsilon_1^{\ddagger}$. For the curves showing the patterns for regions IV-VI, we set $\varepsilon_3^{\ddagger} = 6.5$. The black dashed double-headed arrow along the boundary of regions I and II represents the pattern for the HN model.

For both the MM scheme (without proofreading) and the general KPR scheme, the error was a monotonic function of catalytic rate constant. However, for some other reaction transitions, the KPR scheme can allow for a non-monotonic error variation. This would imply that the minimum error can occur at some intermediate value of the rate constant. Specifically, the variation of the rate constant $k_{2,R}$ (keeping $f_2$ and other rates fixed) leads to three limiting values of the error: $\eta_{\rm L}$ ($k_{2,S} << k_{-1,S}$, $\gamma \approx 1$), $\eta_{\rm M}$ ( $k_{2,S} < k_{-1,S}$, $\gamma >> 1$) and $\eta_{\rm H}$ ($k_{2,S} >> k_{-1,S}$, $\gamma >> 1$ ). Explicit expressions are given by

$$\eta_{\rm L} = f_p f_{-3}\left(\frac{k_{3,R}+k_{p,R}}{k_{3,W}+k_{p,W}}\right);\ \frac{\eta_{\rm L}}{\eta_{\rm M}} = \frac{f_3}{f_{-2}} = e^{\varepsilon^{\ddagger}_{23}};\ \frac{\eta_{\rm H}}{\eta_{\rm M}} = \frac{f_{-1}}{f_2} = e^{\varepsilon^{\ddagger}_{21}};\ \frac{\eta_{\rm H}}{\eta_{\rm L}} = \frac{f_1}{f_{-3}} = e^{\varepsilon^{\ddagger}_{31}}. \qquad (4)$$

Here, $\varepsilon^{\ddagger}_{23} = \varepsilon^{\ddagger}_2 - \varepsilon^{\ddagger}_3$, $\varepsilon^{\ddagger}_{21} = \varepsilon^{\ddagger}_2 - \varepsilon^{\ddagger}_1$ and $\varepsilon^{\ddagger}_{31} = \varepsilon^{\ddagger}_3 - \varepsilon^{\ddagger}_1 = \varepsilon^{\ddagger}_{21} - \varepsilon^{\ddagger}_{23}$. Values of the ratios of these bounds, which are again *controlled only by the transition state energy differences*, lead to six basic patterns of error variation as a function of $k_{2,R}$. The resulting phase diagram of error variation is shown in Fig. 3. The regions I-VI correspond to different relationships of transition state energy differences. Similar non-monotonic patterns are obtained as a function of $k_{-1,R}$ (with fixed $f_{-1}$) but, of course, in an opposite manner (not shown here).

In the HN model, it was assumed that only the dissociation rate constants of the intermediates ($k_{-1,S}, k_{3,S}$, $S = R/W$) are different between the two pathways.[3,7] This leads to $\varepsilon^{\ddagger}_1 = 0 = \varepsilon^{\ddagger}_3$, $\varepsilon^{\ddagger}_2 = \varepsilon_1 = \varepsilon_2$ and subsequently $\eta_{\rm L} = \eta_{\rm H} > \eta_M$. Thus, the pattern exhibited by the HN model lies along the boundary between regions I and II, *i.e.*, along the $\varepsilon^{\ddagger}_{21} = \varepsilon^{\ddagger}_{23} > 0$ line (The black dashed double-headed arrow in Fig. 3).

Next, we consider specific biological proofreading networks to explore which types of error variation patterns may be realized in nature. In the elongation stage of protein translation, ribosome decodes aminoacyl(aa)-tRNAs with high accuracy.[2,15] Detailed kinetic data are available for various steps of the corresponding reaction network in *E. coli*.[10] Specifically, the scheme employed by Zaher *et al.*,[12] focusing on key steps that discriminate between cognate and near-cognate aa-tRNAs, maps nicely into our general KPR scheme shown in

Fig. 2(a). Step-2 in this case is the GTP-hydrolysis step which plays a crucial role in regulating the accuracy[16]. The corresponding data for wild-type(WT) *E. coli* ribosome are listed in Table 1 in SI. We take $k_{-2,R} = k_{-3,R} = 10^{-3}\, s^{-1}$ to ensure that both step-2 and step-3 are nearly irreversible.[12] As $f_{-1} > f_2$ (see Table 1 in SI), according to Eq.(4), $\eta_{\rm M}$ *is always less than* $\eta_{\rm H}$. This suggests that patterns belonging to regions III-V are absent for this system. The limit $\eta_{\rm L}$ depends on the choice of the free parameter $f_{-2}$ ($f_{-3}$ then gets fixed by the constraint of equal $\Delta\mu$). It follows from Eq.(4) that, for $\frac{f_2 f_3}{f_{-1}} < f_{-2} < f_3$, the qualitative pattern of error variation belongs to region I in Fig. 3. According to the data for WT ribosome, this means a broad range of $f_{-2}$ ($4 \times 10^{-3} - 7.9$) over which the system will show such a pattern. For $f_{-2} < \frac{f_2 f_3}{f_{-1}}$, the pattern shifts to that in region II. In contrast, for $f_{-2} > f_3$, the pattern belongs to region VI. These features are verified by the plots shown in Fig. 4(a). However, one does not expect $f_{-2}$ to be significantly greater than one. So, the system is more likely to show patterns of either region I or II. For the sake of completeness, we mention that, as $f_p < f_3$, the minimum in error as a function of the catalytic rate constant (with fixed $f_p$) is obtained in the $k_{p,R} \to 0$ limit.

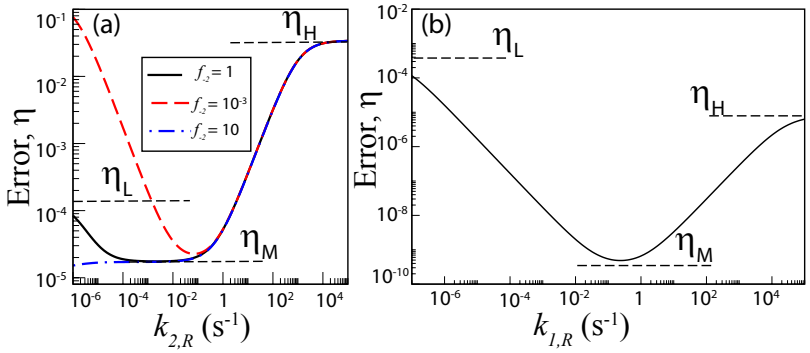


Figure 4: (a) Changes of error, $\eta$ for WT *E. coli* ribosome as a function of the hydrolysis rate constant $k_{2,R}$ for three different choices of $f_{-2}$. Error varies between the bounds as predicted in Eq.(4) (shown for the $f_{-2} = 1.0$ case). (b) Variation of error as a function of the polymerization rate constant $k_{1,R}$ for DNA replication by T7 DNAP enzyme.

We apply a similar approach to the KPR network for the DNA replication in bacteriophage T7 by T7 DNA polymerase (DNAP) enzyme.[11] Here, variation of the polymerization rate constant $k_{1,R}$ results in three bounds of errors similar to the GTP hydrolysis step in

the tRNA selection (for detailed expressions, see SI). Our calculations predict that for this system the transition state energy differences also govern the pattern of error variation. Corresponding kinetic data[17] (see Table 2 in SI) imply that the pattern should be qualitatively similar to that for region II in Fig. 3. The plot in Fig. 4(b) shows that this is indeed the case.

In this study, we developed a quantitative theoretical method to investigate the mechanisms of selectivity in biological processes. More specifically, we investigated how the free energy landscapes control the enzymatic selectivity error. To this end, the MM scheme and the Hopfield-Ninio KPR reaction scheme were analyzed for a general set of parameters without any simplifying assumptions on the rate constants. For both schemes, the values of error are shown to only depend on the values of the transition state energies and invariant to changes in energy of stable enzyme-substrate complexes. Moreover, we showed that the error changes monotonically as a function of the catalytic rate constants and the sign of the change is given by the differences in the transition state energy values. Thus, the highest selectivity limit (lowest error) is *always* determined by kinetic discrimination. Therefore, in general, the error correction, with or without proofreading, is fully determined by kinetic discrimination factors. Thermodynamic discrimination arises only as a special case when the kinetic and thermodynamic discrimination factors coincide. Furthermore, in our generalized KPR network, we find that error can be non-monotonic function of the rates of other reaction steps. The pattern of error variation in such cases is again governed by transition state energy differences, and multiple behaviors can be found. Taking important biological KPR networks as guiding examples, we show which type of error variation patterns are present in living systems. Thus, this theoretical analysis clarifies some important features of the enzymatic selectivity mechanisms in biological systems.

## Acknowledgement

This work is supported by Center for Theoretical Biological Physics NSF Grant PHY-1427654. ABK also acknowledges the support from the Welch Foundation (Grant C-1559) and from the NSF (Grant CHE-1360979).

## References

(1) Kunkel, T. A.; Bebenek, K. DNA Replication Fidelity. *Annu Rev Biochem* **2000**, *69*, 497–529.

(2) Zaher, H. S.; Green, R. Fidelity at the Molecular Level: Lessons from Protein Synthesis. *Cell* **2009**, *136*, 746–762.

(3) Hopfield, J. J. Kinetic Proofreading: A New Mechanism for Reducing Errors in Biosynthetic Processes Requiring High Specificity. *Proc Natl Acad Sci USA* **1974**, *71*, 4135–4139.

(4) Bennett, C. H. Dissipation-error tradeoff in proofreading. *BioSystems* **1979**, *11*, 85–91.

(5) Sartori, P.; Pigolotti, S. Kinetic versus energetic discrimination in biological copying. *Phys Rev Lett* **2013**, *110*, 188101.

(6) Murugan, A.; Huse, D. A.; Leibler, S. Speed, dissipation, and error in kinetic proofreading. *Proc Natl Acad Sci USA* **2012**, *109*, 12034–12039.

(7) Hartich, D.; Barato, A. C.; Seifert, U. Nonequilibrium sensing and its analogy to kinetic proofreading. *New J Phys* **2015**, *17*, 055026.

(8) Ninio, J. Kinetic amplification of enzyme discrimination. *Biochimie* **1975**, *57*, 587–595.

(9) Hopfield, J. J.; Yamane, T.; Yue, V.; Coutts, S. M. Direct experimental evidence for

kinetic proofreading in amino acylation of tRNAIle. *Proc Natl Acad Sci USA* **1976**, *73*, 1164–1168.

(10) Gromadski, K. B.; Rodnina, M. V. Kinetic Determinants of High-Fidelity tRNA Discrimination on the Ribosome. *Mol Cell* **2004**, *13*, 191–200.

(11) Johnson, K. a. Conformational coupling in DNA polymerase fidelity. *Annu Rev Biochem* **1993**, *62*, 685–713.

(12) Zaher, H. S.; Green, R. Hyperaccurate and Error-Prone Ribosomes Exploit Distinct Mechanisms during tRNA Selection. *Molecular Cell* **2010**, *39*, 110–120.

(13) van Kampen, N. G. *Stochastic processes in physics and chemistry*, 3rd ed.; North Holland Publishing Company, Amsterdam, 2007.

(14) Kolomeisky, A. B. *Motor Proteins and Molecular Motors*; CRC Press, Taylor and Francis Group, 2015.

(15) Johansson, M.; Zhang, J.; Ehrenberg, M. Genetic code translation displays a linear trade-off between efficiency and accuracy of tRNA selection. *Proc Natl Acad Sci USA* **2012**, *109*, 131–136.

(16) Wohlgemuth, I.; Pohl, C.; Mittelstaet, J.; Konevega, A. L.; Rodnina, M. V. Evolutionary optimization of speed and accuracy of decoding on the ribosome. *Phil Trans R Soc B* **2011**, *366*, 2979–2986.

(17) Wong, I.; Patel, S. S.; Johnson, K. A. An induced-fit kinetic mechanism for DNA replication fidelity: direct measurement by single-turnover kinetics. *Biochemistry* **1991**, *30*, 526–537.